Phosphoric Acid Pre-treatment to Tailor Polybenzimidazole Membranes for Vanadium Redox Flow Batteries

Sandip Maurya[1*], Sergio Diaz Abad[1], Eun Joo Park[1], Kannan Ramaiyan[1,#], Yu Seung Kim[1], Benjamin L Davis[1], Rangachary Mukundan[1*]

[1]MPA-11: Materials Physics Applications, Los Alamos National Laboratory, Los Alamos, NM, 87545, USA

[#]Current affiliation: Advanced Materials Lab, Department of Chemical & Biological Engineering, University of New Mexico, Albuquerque, 87131, USA

Abstract:

Vanadium redox flow batteries (VRFBs) use ion-selective membranes for transporting ionic species while separating the positive and negative electrolytes. In this paper, we report phosphoric acid doped polybenzimidazole (PBI) membranes that yield high ionic selectivity and conductivity in VRFBs. The phosphoric acid pre-treatment swells the PBI matrix irreversibly and increases its sulfuric acid doping in VRFB electrolytes. The pre-treated membranes show comparable area resistance with Nafion-212 with better selectivity towards vanadium ions. A low resistance was obtained with a reduced membrane thickness, which can reduce the overall cost of materials. The VRFB using an optimized phosphoric acid pre-treated PBI membrane demonstrates coulombic, voltage, and energy efficiencies of 99.7, 90.3, and 90.0%, respectively, at 40 mA cm^{-2} while achieving ~40% higher discharge capacity compared to Nafion-212. Furthermore, the VRFB cell shows excellent cycling stability, i.e., only 6.8% or 0.068% per cycle capacity decay for 100 cycles while maintaining coulombic efficiency at >99.9% (98.5% coulombic efficiency for Nafion-212 with a capacity decay of 0.42% per cycle) proving the effectiveness of pre-treatment of phosphoric acid on PBI membranes.

* Corresponding authors: smaurya@lanl.gov, mukundan@lanl.gov

1. Introduction:

A redox flow battery is fundamentally like fuel cells, utilizing aqueous anolyte solution instead of hydrogen or alcohols as fuels, and catholyte solution instead of oxygen or air as an oxidant [1]. In the case of Vanadium redox flow batteries (VRFBs), the electrolyte solution containing different valences of vanadium in the anolyte and catholyte is separated by a membrane. Due to their independent power output and energy capacity, VRFBs are easily scalable and therefore suitable for large-scale energy storage applications. Perfluorosulfonic acid (PFSA) membranes such as Nafion have been the membrane of choice for state-of-the-art VRFB systems due to their high ionic conductivity and stability in extremely oxidative electrolyte solutions. However, due to the poor selectivity towards vanadium ions that results in rapid capacity loss and thus low energy efficiency, VRFBs with PFSA membranes need frequent electrolyte balancing; for instance, a Nafion membrane loses about 60% of capacity within 100 cycles [2]. In addition, the high cost of PFSA membranes further motivates researchers to replace them with more cost-effective hydrocarbon membranes; even when mass produced Nafion membranes would cost at least \$500/m^2 vs. \$20/m^2 for hydrocarbon membranes [3-5].

Several groups have synthesized sulfonated hydrocarbon-based cation exchange membranes, including poly(phthalazinone ether sulfone ketone) [6], poly(ether ether ketone) [7], poly(fluorenyl ether ketone) [8], poly(arylene thioether) [9] and composites of Nafion [10] for VRFBs. Although good performance was observed in VRFBs, they showed poor selectivity for vanadium ions over protons and suffered from crossover due to the cationic nature of sulfonic acid. Recently, the use of anion exchange membranes is gaining popularity since the positive charge fixed in the membrane repels the positively charged vanadium ions and subsequently suppresses their crossover [11, 12]. As a result, high energy efficiencies along with a longer duration between electrolyte rebalancing can be achieved. However, the chemical stability of the quaternized hydrocarbon membranes is questionable in strong oxidative solutions of VO_2^+ present in VRFBs. In particular, aryl-ether linkages in widely used polyphenylene oxide and quaternary ammonium groups of anion exchange membrane are prone to oxidative attack, which causes molecular weight decrease and loss of cationic functional groups of the polymers [13-15]. As a result, the membranes lose their mechanical and electrochemical properties, leading to higher resistance and crossover in VRFBs [16].

Recent works have shown that polybenzimidazole (PBI) may be a suitable membrane for VRFBs. PBI has features that make it a promising alternative to Nafion, such as excellent chemical

and mechanical properties, and low-cost [17, 18]. PBI is a basic polymer that can strongly interact with acids through hydrogen bonding to become proton conductive [19]. In addition, PBI does not contain any oxidation-prone linkages in its polymer backbone that makes it survive under highly oxidative conditions and retain 90% of its weight over a period of 7 days in the Fenton solution [20]. PBI membranes were first used in VRFBs by Zhou et al., demonstrating excellent properties, including low VO^{2+} crossover and high coulombic efficiency of nearly 100% [21]. However, the conductivity of PBI is lower compared with that of Nafion, leading to low voltage and energy efficiencies at higher current densities. To increase the ionic conductivity of PBI, some studies have reported modification of the PBI backbone to enhance its intrinsic conductivity or increase the free volume of the membrane to reach higher acid doping levels [22-25]. Apart from backbone modifications, researchers have also focused on membrane fabrication methods, such as blending PBI with polymers with higher ionic conductivity [26-28], preparing composite membranes where PBI acts as a matrix blocking the crossover of vanadium ions [29-31], or porous PBI membranes where pores are filled with the electrolyte providing high conductivity [32-34]. A simple method to increase sulfuric acid doping level was reported by Peng et al., [35] where the PBI membrane was pre-treated with phosphoric acid before being assembled into the VRFB cell. A pre-treatment step was performed by immersing the PBI membrane into 85 wt% phosphoric acids, followed by immersion in 3 M sulfuric acid. The pre-treatment with phosphoric acid increased the free volume of the PBI membrane, which resulted in higher sulfuric acid uptake and higher conductivity while maintaining low permeability. However, the swelling of the pre-treated membrane was excessive, and as a result, the long-term cycling showed poor performance with a 20% capacity loss in the first 20 cycles at 50 mA cm^{-2}.

In this study, we applied a pre-treatment strategy whereupon PBI is doped with phosphoric acid to tailor the membrane properties for better VRFB performance. To study the effects of phosphoric acid doping, we used three different concentrations (5, 10 and 15 M) for doping of the PBI membranes. In addition, membranes two different thicknesses (25 and 65 μm) were pre-treated with phosphoric acids to optimize conductivity and crossover in VRFBs. Subsequently, we characterized the PBI membranes for their physicochemical properties, vanadium crossover and VRFB performance and compared them with the commercially available Nafion-212 membrane.

2. Experimental:

2.1 Materials

The Celazole® PBI polymer was obtained in the form of membrane from PBI Performance Products, Inc., USA. The vanadium (IV) oxide sulfate hydrate (97%), sulfuric acid solution (2.5 M), phosphoric acid (85 wt%), magnesium sulfate (98%) and *N,N*-dimethylacetamide (DMAc, anhydrous) were purchased from Sigma-Aldrich. The acids were diluted using deionized water obtained from Millipore® deionized water purification system producing water at 18.2 MΩ·cm. All the chemicals were of analytical grade and used without further purification.

2.2 Preparation of phosphoric acid doped PBI membranes

A calculated amount of the PBI polymer (8 wt%) was dissolved in DMAc at 80 °C to make a homogeneous solution. The polymer solution was cast on a glass plate using a doctor blade followed by drying of solvent in a conventional oven at 80 °C for 6 h. The thin film was peeled from the glass plate and its thickness was recorded. The membranes with dry thicknesses of 25 ± 3 were casted in the lab. The membranes with thickness of 65 ± 4 μm were purchased from PBI Performance Products, Inc. and used as received.

Membranes with fixed size (8 cm × 8 cm) were doped with phosphoric acid (5, 10 and 15 M) for 72 h at room temperature to prepare phosphoric acid doped PBI membranes. The doped membranes were wiped with filter paper to remove excess phosphoric acid from the surface prior to swelling and thickness measurements. Then, phosphoric acid doped membranes were immersed in 2.5 M sulfuric acid to exchange the phosphoric acid with sulfuric acid. After wiping excess sulfuric acid from the surface, thickness, swelling ratio and sulfuric acid uptake were measured before using as a separator in VRFBs. The membranes were denoted as P/x/y where P is PBI, x is the base membrane thickness in μm, and y is the phosphoric acid concentration at which membranes were treated. For example, P/65/5 stands for the PBI membrane with 65 μm thickness treated with 5 M phosphoric acid.

2.3 Membrane physical characterizations

Elemental composition of fresh and phosphoric acid doped membranes was measured using Energy Dispersive X-Ray Spectroscopy (EDS) attached to the Scanning Electron Microscope (FEI Quanta 45 SEM) with an accelerating voltage of 5 kV. Membrane samples were prepared by doping with phosphoric acid and sulfuric acid exchange as mentioned in section 2.2. Samples for EDS were prepared by freeze-fracturing using liquid nitrogen, and EDS mapping was performed on membrane cross-sections without gold or platinum sputtering.

The swelling ratio of the membranes was measured by a linear expansion of dry and wet thickness of membrane samples before and after immersing in 2.5 M sulfuric acid or 85% phosphoric acid. The calculation was based on the following equation:

$$\text{Swelling ratio (\%)} = [(l_{wet} - l_{dry}) / l_{dry}] \times 100\%$$

where l_{dry} and l_{wet} are the length of diameter of dry and wet samples, respectively.

The acid uptake of PBI membranes was measured using 2.5 M sulfuric acid solution and it was calculated based on the following equation:

$$H_2SO_4 \text{ uptake (\%)} = [(W_{wet} - W_{dry}) / W_{dry}] \times 100\%$$

where W_{dry} and W_{wet} are the Weight of dry and wet samples, respectively.

The proton conductivity of membranes were calculated from the high frequency resistance obtained from the single cell VRFB using below equation:

$$\text{Proton conductivity (mS cm}^{-1}) = \frac{l\ (cm)}{R\ (\Omega\ cm^2)} \text{ x } 1000$$

where l and R are the thickness and membrane resistance, respectively.

2.4 Vanadium ion permeability

The vanadium ion permeability test was conducted in a diffusion cell at room temperature. The cell consists of two chambers of 20 ml volume, and the area of membrane was 1.5 cm^2. One compartment was filled with 1 M $VOSO_4$ in 2.5 M H_2SO_4 solution, and the other compartment was filled with 1 M $MgSO_4$ in 2.5 M H_2SO_4 solution. $MgSO_4$ was used to balance the osmotic pressure generated by $VOSO_4$. The migration of vanadium ions was analyzed by UV-VIS spectroscopy by scanning at 765 nm. The vanadium ion permeability coefficient was calculated using the below equation:

$$V \frac{dC_B(t)}{dt} = A \frac{P}{L} (C_A - C_B(t))$$

where V is the solution volume in each chamber, A is effective membrane area, P is permeability, L is thickness of membrane, C_A is vanadium ion concentration in $VOSO_4$ chamber, $C_B(t)$ is the vanadium ion concentration in $MgSO_4$ chamber at time t, and $\frac{dC_B(t)}{dt}$ is the change in vanadium concentration in $MgSO_4$ chamber as a function of time.

2.5 Performance evaluation in VRFB

The single VRFB cell was assembled as reported elsewhere [36]. The phosphoric acid pre-treated membrane (7.62 x 7.62 cm^2, effective membrane area of 25 cm^2) was sandwiched between thermally treated graphite felt electrodes (5 x 5 cm^2, SGL carbon GFD 4.6EA, 500 ^oC, 5 h). The membrane electrode assembly was further placed between two impervious bipolar plates with 1.75 mm deep square trench (5 x 5 cm^2, densified and resin-filled graphite plates, graphitestore Inc.). The gold-plated copper current collectors were placed on both sides of the bipolar plates, and end plates were used to finish cell assembly. The VRFB test was started with 120 mL and 60 mL of 1.0 M $VOSO_4$ in 2.5 M H_2SO_4 electrolyte in the positive (catholyte) and negative (anolyte) reservoirs, respectively. The electrolyte flowrate was 40 mL min^{-1} and the VRFB was charged at a constant voltage of 1.8 V until current reached 50 mA; after that 60 mL of catholyte was removed. The polarization curves were measured using the DC electronic load box (Keysight 3300 series equipped with EIS capability) from open circuit voltage (~100% state of the charge (SOC)) to 0.2 V with 0.1 V step for 5 seconds. The state of the charge (SOC) was determined from the open circuit voltage (OCV) of the cell. The VRFB cycling tests were carried out between 40 – 200 mA cm^{-2} with an interval of 40 mA cm^{-2} and a total of 5 cycles were carried out for each current density. The single cell was charged/discharged between 1.8 and 0.8 V using a battery cycler (Scribner flow battery station). Argon was constantly purged to remove atmospheric oxygen from the electrolyte reservoir. The coulombic efficiency (CE), voltage efficiency (VE) and energy efficiency (EE) were calculated using the below equations:

$$CE = \frac{\int I_{discharge}\,\mathrm{dt}}{\int I_{charge}\,\mathrm{dt}} \times 100\%$$

$$EE = \frac{\int \left(V_{discharge} \times I_{discharge}\right)\mathrm{dt}}{\int \left(V_{charge} \times I_{charge}\right)\mathrm{dt}} \times 100\%$$

$$VE = \frac{EE}{CE} \times 100\%$$

where I is current, V is voltage and t is time during the charge-discharge cycling.

3. Results and Discussions:

3.1 VRFB performance using untreated PBI membrane

The performance of the untreated PBI membranes was assessed as a function of membrane thickness. The charge/discharge curves of the flow cell assembled with two different thicknesses of PBI membranes (25 and 65 μm) are shown in Fig. S1 (supporting information). As expected, the overpotential increases with the increase in membrane thickness, for instance, P/65/0 displays a higher voltage gap of 102 mV at 40 mA cm^{-2} and 344 mV at 80 mA cm^{-2} when compared with charge/discharge curves of P/25/0. The P/25/0 membrane shows lower overpotential due to its low resistance, which results in higher VE and EE. The CE, VE, and EE at 40 mA cm^{-2} are 99.8%, 84.3%, 84.2% and 99.3%, 67.7%, 67.2% for P/25/0 and P/65/0, respectively. The EE of P/25/0 and P/65/0 at different current densities are presented in Table S1 (supporting information). It is worth noting that the low resistance allows for the operation of the P/25/0 membrane at a higher current density, on the other hand, the current density is limited to 80 mA cm^{-2} for the P/65/0 membrane. Moreover, CE over 99% indicates the extremely low crossover of vanadium ions through the PBI membranes without any treatment owing to positively charged benzimidazolium groups in acidic electrolytes [21].

Polarization measurements can attribute voltage losses to either activation loss, *iR* (ohmic) loss, or concentration or mass-transport limitation. As shown in Fig. 1, P/25/0 and P/65/0 produce peak power densities of 0.34 and 0.10 W cm^{-2}, respectively. The low peak power densities for P/65/0 emphasize the significance of ohmic losses associated with higher membrane thickness. For instance, the cell voltages at 0.238 A cm^{-2} were 0.213 V and 0.890 V, respectively, for P/25/0 and P/65/0 membranes. These results are in good agreement with the charge/discharge cycling test where the P/65/0 membrane could only be cycled up to 80 mA cm^{-2} due to higher membrane resistance, and as a result, the VRFB cell reaches the cut-off voltage limit quickly (Table S1, supporting information). The *iR*-free current-voltage (IV) curves in Fig. 1 also indicate that voltage losses are predominantly due to the ohmic overpotential associated with the membrane resistance. The P/25/0 membrane with lower resistance (0.91 **Ω** cm^2 vs. 3.77 **Ω** cm^2 of P/65/0) was charged/discharged at higher current densities without hitting cut-off voltage limits, eventually extending charge/discharge time as a result charge/discharge capacity. Therefore, P/25/0 achieves a higher charge/discharge capacity of 9.57/9.56 Ah L^{-1} at 80 mA cm^{-2} whereas P/65/0 only achieved 3.69/3.65 Ah L^{-1} – about 60% less discharge capacity.

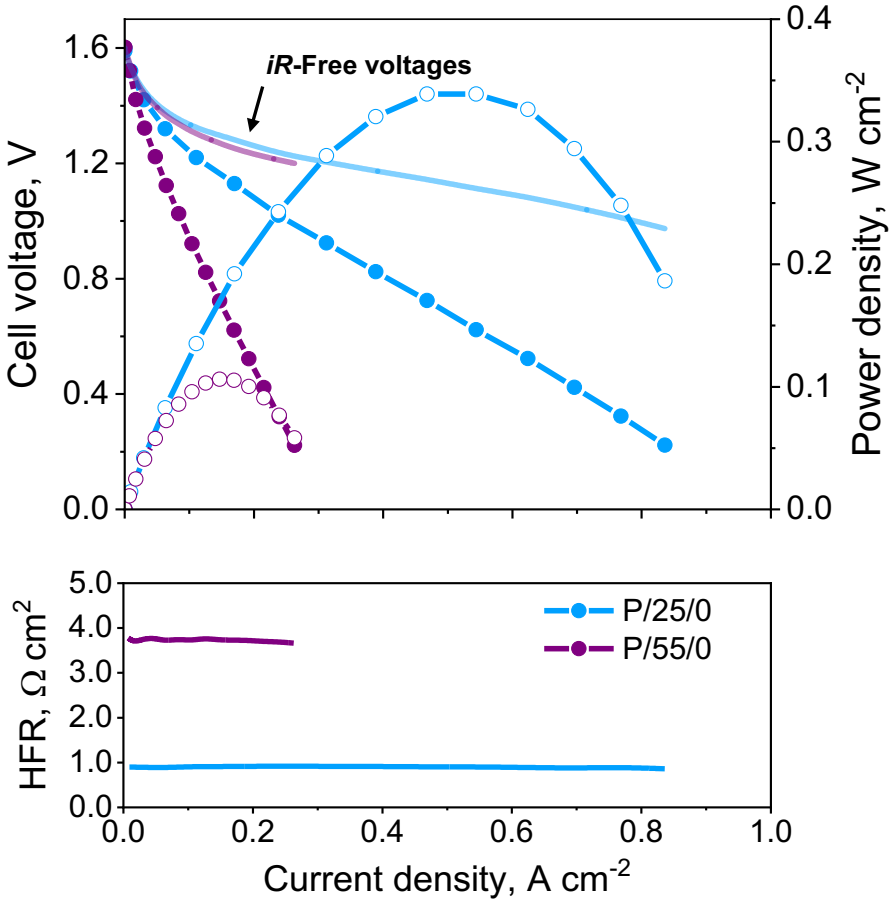

Figure 1. Polarization curves of the VRFBs assembled with the untreated P/25/0 and P/65/0 membranes (flow rate: 60 mL min^{-1}).

3.2 Properties of phosphoric acid pre-treated PBI membranes

In this study, all PBI membranes were immersed in phosphoric acid solutions for 72 h. The thickness and swelling ratio in phosphoric acid solutions, and after exchanging phosphoric acid with sulfuric acid, to mimic the VRFB electrolyte condition, were measured. Acidic electrolytes, including phosphoric acid (pK_{a1} = 2.16), will react with the Lewis base imidazole sites in PBI (pK_a = 5.5) [37]. The resulting benzimidazolium cations allow the modified PBI membrane to be selective toward anions, which is a desirable quality for VRFBs. The PBI membrane can achieve acid doping levels as high as 7.2 phosphoric acids per benzimidazole within 72 h at ambient conditions, where 95% of it was achieved within the first 24 h [35]. Whereas, the concentrated

sulfuric acid solutions provide the doping level of 2 for PBI, *i.e.,* two acid molecules per repeating unit or benzimidazole group vs. 7.2 with phosphoric acid [35]. The higher doping level in phosphoric acid treated PBI is attributed to extended hydrogen bond forming ability of phosphoric acid that induces higher swelling in PBI matrix (Fig. 2). Immersion of phosphoric acid pre-treated PBI membranes in sulfuric acid not only changes its transport properties but also induces a permanent swelling resulting in higher acid uptake.

Table 1. Physical properties of Nafion-212 and acid doped PBI membranes.

Membrane	Thickness, μm		Swelling ratio, %		H_2SO_4 uptake, %	VO^{2+} Permeability, 10^{-7} cm^2 min^{-1}	Proton Conductivity, mS cm^{-1}
	H_3PO_4	H_2SO_4	H_3PO_4	H_2SO_4			
P/65/0	-[a]	70	-[a]	9.1	56.4	0[b]	1.6
P/65/5	78	71	23.6	14.5	66.7	0[b]	1.8
P/65/10	91	85	47.3	36.4	82.1	5.8	3.3
P/65/15	103	93	67.3	50.9	142.3	60.3	17.3
Nafion-212	-[a]	58	-[a]	9.8	8.7	64.2	12.0

[a] not treated with phosphoric acid, [b] not measurable

Table 1 presents the physical properties of acid-doped PBI membranes. PBI membranes are known to swell anisotropically in-plane and thickness directions due to the specific orientations of PBI chains [35]. The as-received PBI membrane with 65 μm thickness swells to 78, 91, and 103 μm when immersed in 0 (only immersed in 2.5 M sulfuric acid), 5, 10, and 15 M (85 wt%) phosphoric acid, respectively. The membrane thickness was reduced to 70, 71, 85, and 93 μm after immersing in 2.5 M sulfuric acid for 24 hours which gave a swelling ratio of 9.1, 14.5, 36.4, and 50.9 for P/65/0, P/65/5, P/65/10 and P/65/15 membranes, respectively. The phosphoric acid treatment at a higher concentration significantly increased the membrane swelling after phosphoric acid was replaced with sulfuric acid indicating a higher free volume. Therefore, the cross-section of PBI membranes was examined to visualize any effects of phosphoric acid treatment on membrane morphology (Fig. S2a, supporting information). It is evident from the cross-sections of P/65/0, P/65/5, P/65/10, and P/65/15 that the phosphoric acid treatment increases the membrane thickness, but no porosity formation was observed. Moreover, EDS mapping shows a quick replacement of phosphoric acid by sulfuric acid due to the absence of a phosphorous peak in the elemental map (Fig. S2b, supporting information).

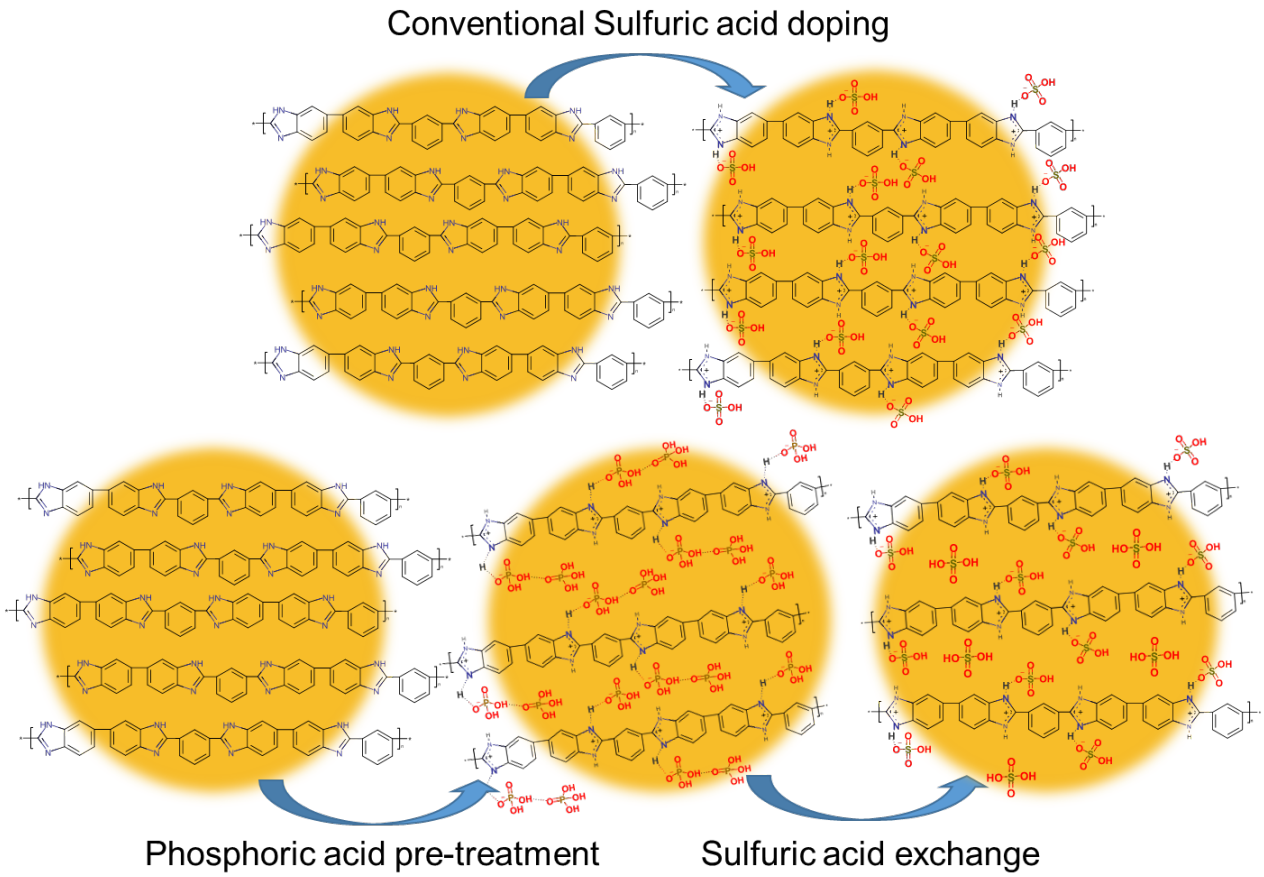

Figure 2. The pre-treatment strategy for the PBI membrane.

The sulfuric acid doping level and uptake do not change when sulfuric acid concentration is increased [38]. Therefore, our pre-treatment of PBI membranes with phosphoric acid followed by sulfuric acid is particularly advantageous as it can increase the sulfuric acid uptake ~ 2.5 times (Table 1). The VO^{2+} permeability of acid-doped PBI and Nafion-212 membranes are presented in Table 1. The P/65/0 and P/65/5 membranes did not show any measurable crossover after 7 days (~170 h), which is also consistent with the literature [39]. The P/65/10, P/65/15, and Nafion-212 membranes show vanadium permeability of 5.8×10^{-7}, 60.3×10^{-7}, and 64.2×10^{-7} cm^2 min^{-1}, respectively. The vanadium permeability of the Nafion-212 membrane is in good agreement with the values reported in the literature *i.e.* 41×10^{-7} by Wang et al. [40]. In general, ion-selective membranes have non-diffusible fixed ionic groups (either anionic or cationic), which repel like charges, restricting diffusion through the membrane. This electrostatic repulsion results in ion selectivity for membranes, which is known as the Donnan effect [41]. A clear improvement is observed in conductivity with the phosphoric acid pre-treatment as it increases the conductivity of

PBI membranes from 1.6 mS cm^{-1} to 17.3 mS cm^{-1}. The increase in the conductivity could be attributed to the higher sulfuric acid uptake. It should also be noted that the higher sulfuric acid uptake due to the larger free volume improves the membrane conductivity at the expense of selectivity, evident from the permeability, due to the weaker Donnan effect.

3.3 VRFB performance using phosphoric acid pre-treated PBI membrane

To investigate the effect of phosphoric acid treated PBI membranes on the VRFB performance, the discharge polarization curves of P/65/15 and Nafion-212 are shown in Fig. 3. The high-frequency resistance (HFR) is 0.54 and 0.48 Ω cm^2 for P/65/15 and Nafion-212, respectively. The peak power densities of P/65/15 and Nafion-212 are 0.57 W cm^{-2} (0.81 V) and 0.58 W cm^{-2} (0.67 V), respectively, at ~100% SOC and 60 mL min^{-1}. The discharge polarization curves are significantly different in the mass transport region (at high current density) where Nafion-212 shows lower polarization losses than P/65/15 membrane. The P/65/15 membrane could only achieve lower discharge capacity 6.1 Ah L^{-1} (whereas Nafion-212 achieved discharge capacity of 8.1 Ah L^{-1}). Therefore, during the polarization curve measurement the cell using P/65/15 membrane was quickly starved of the charged electrolyte and hence showed mass transport limitation at higher current density. The polarization curve for P/65/10 membrane shows no mass transport losses as it is dominated by ohmic losses due to lower conductivity than P/65/15 (Fig. S3, supporting information). The polarization curves of phosphoric acid pre-treated PBI membrane show comparable peak power density in VRFBs, suggesting that PBI membranes could be a less expensive alternative for VRFBs.

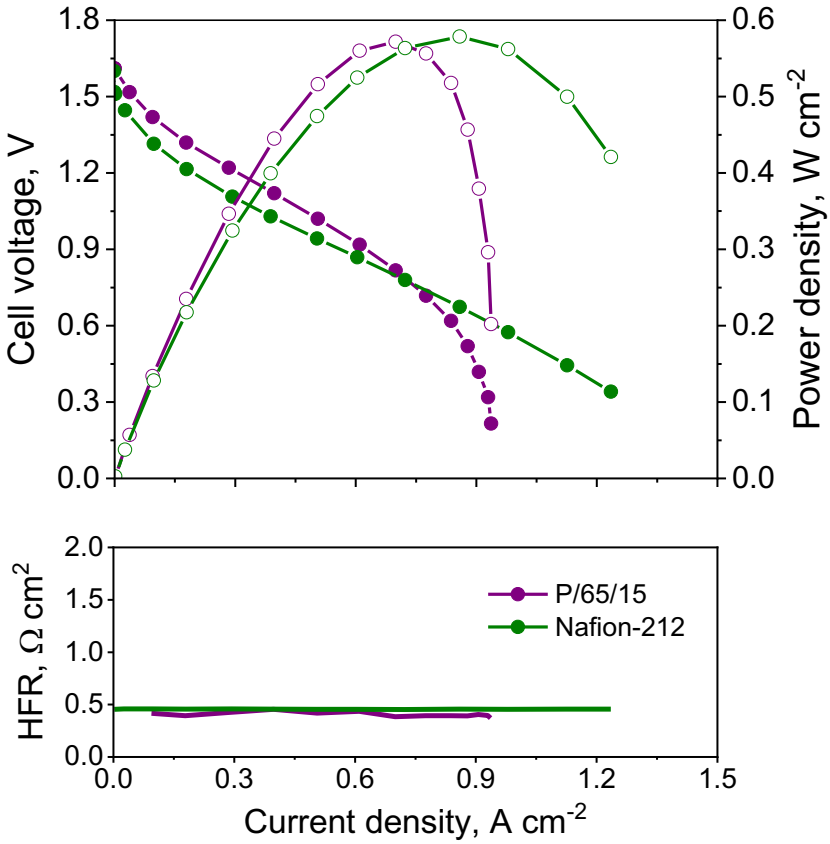

Figure 3. Polarization curves of the VRFBs assembled with P/65/15 and Nafion-212 membranes (flow rate: 60 mL min^{-1}).

We tested the pre-treated PBI membranes in a single cell at current densities from 40 to 200 mA cm^{-2} to compare VRFB performance with the Nafion-212 membrane. As shown in Fig. 4a, P/65/15 shows poor CE when compared with P/65/5, P/65/10, and other undoped PBI membranes reported in the literature [22, 42]. It is attributed to the high swelling ratio of P/65/15, which results in high permeability for VO^{2+} ions. Though higher free volume due to swelling improves the overall conductivity of P/65/15, the EE values are lower than the Nafion-212 membrane at low current densities (70.2% vs 86.3% at 40 mA cm^{-2}) due to excessive vanadium crossover during the charge/discharge cycles. For all membranes, an increase in cycling current density increases the CE due to shorter cycling times, which reduces the time for vanadium ions to crossover during each cycle. P/65/5 shows the highest possible CE of ~ 100% at 40 and 80 mA cm^{-2}. P/65/5 cannot be cycled at higher current densities due to the higher membrane resistance,

which is evidenced by the low VE at 80 mA cm^{-2} (59%). The P/65/10 membrane shows the most promising VRFB performance, as free volume expansion by the pre-treatment step allowed a considerable proton conductivity increase. P/65/10 membrane performs better than the commercial Nafion-212 membrane, demonstrated by a superior EE of ca. 87.5% compared with 86% of Nafion-212 at 40 mA cm^{-2}. P/65/10 membrane also shows discharge capacities of ~23% and ~17% higher than the Nafion-212 membrane at 40 and 80 mA cm^{-2}, respectively. It should also be noted that Nafion-212 outperforms PBI membranes at high current densities in terms of not only efficiencies but also discharge capacities. It is attributed to the fact that both Nafion-212 and PBI membranes conduct protons differently, Nafion-212 contains well-formed ionic nanochannels for proton conduction, while the proton conduction mechanism is less known for PBI membranes in an aqueous environment. For instance, the VE for Nafion-212 was 16% lower at 200 mA cm^{-2} compared to 40 mA cm^{-2}, whereas it was 40% lower for P/65/10 membrane. Therefore, it is evident that optimization with the PBI membrane is necessary to further improve the VRFB performance.

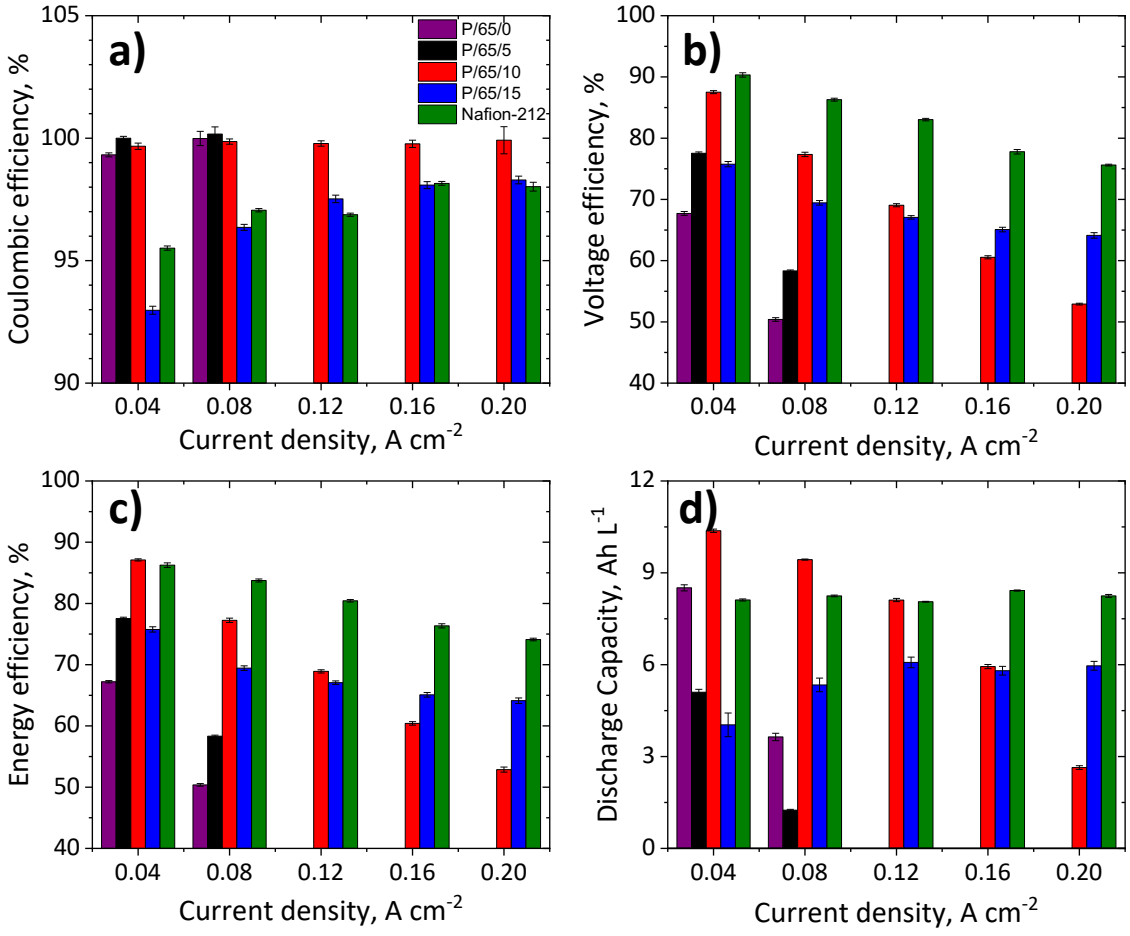

Figure 4. Average VRFB energy efficiencies and discharge capacities at different current densities for Nafion-212 and pre-treated PBI membranes (Flow rate: 40 mL min^{-1}).

For the P/65/y membranes, we found that the optimum phosphoric acid concentration for the pre-treatment step is 10 M, creating sufficient free volume to be filled with the acid electrolyte but not too high to allow large vanadium crossover. Far superior performance was obtained for the thinner PBI membranes due to the lower resistance, as shown in Fig. 1. Therefore, to optimize the PBI membranes for VRFB, pre-treatment was carried out on PBI membranes with a base thickness of 25 μm. The P/65/15 and P/25/15 membranes exhibited very high vanadium crossover, owing to the large swelling, which makes them unsuitable for VRFB operations. The physical properties of P/25/y membranes are presented in Table S2. As shown in Fig. 5, P/25/5 and P/25/10 membranes show CE > 99% at all current densities, indicating the effectiveness of phosphoric acid pre-treatment on thinner membranes. Nevertheless, the VE of the Nafion-212 membrane is still high, but P/25/y membranes showed comparable VE at lower current densities. P/25/y membranes show higher EE at a lower current density than that of the Nafion-212, and the trend starts to reverse at current densities higher than 80 mA cm^{-2}. For instance, EE of the P/25/5, P/25/10, and Nafion-212 membranes were measured to be 90.1, 89.1, and 86.3% at 40 mA cm^{-2}, 77.6, 78.2, and 80.4% at 120 mA cm^{-2}, and 68.1, 70.7, and 74.1 at 200 mA cm^{-2}, respectively. The VRFB efficiencies do not always display the full picture as the crucial parameter "discharge capacity" is often kept hidden from plain sight in literature. For example, the P/25/5 membrane shows EE of 68.1% (vs. 74.1% of Nafion-212) at 200 mA cm^{-2} but still shows remarkably ~40% and 18% higher discharge capacity than that of the Nafion-212 at 40 and 200 mA cm^{-2}, respectively. The VRFB performance of P/25/y membranes were also compared to thinner Nafion-211 membrane where P/25/y membrane shows equivalent energy efficiency at lower current densities such as 40 mA cm^{-2}, however, it is obvious and also reported in literature that thinner Nafion-211 membrane loses its capacity much faster than its thicker counterparts due to excessive vanadium crossover [43]. The discharge capacity should increase with increasing current density due to the lesser time available for vanadium crossover. This is true for the Nafion-211 and P/65/15 case. However, the higher resistance of the thicker membrane will also result in a decrease in discharge capacity due to ohmic losses. This is the case for Nafion-117 as shown in Fig. S4 and all other pre-treated PBI membranes. In Nafion-212 case, these two factors are roughly balanced to yield an almost constant discharge capacity with varying current during our VRFB testing. These results indicate that the

performance of VRFB utilizing PBI membranes is superior to that of Nafion-212 membranes, with PBI membranes performing better than Nafion-212 at low current densities and exhibiting higher discharge capacities at all current densities.

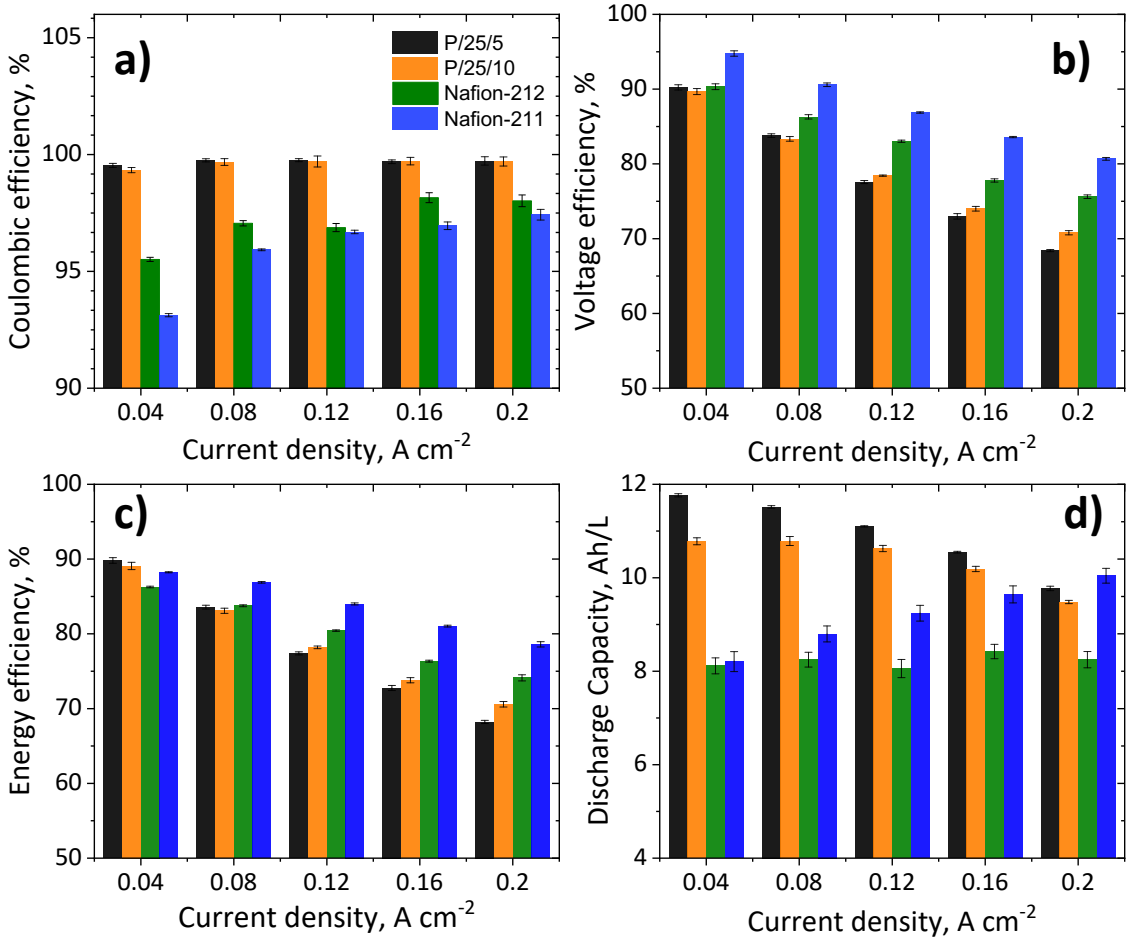

Figure 5. Average efficiencies and discharge capacities obtained in the VRFB at different current densities for P/25/0, P/25/5, P/25/10, P/25/15, Nafion-211, and Nafion-212 membranes (flow rate: 40 mL min^{-1}).

The long-term cycling performance of P/65/15, P/65/10, P/25/5, and Nafion-212 membranes at 80 mA cm^{-2} are shown in Fig. 6. The lower CE of P/65/15 and Nafion-212 are due to their higher vanadium ion permeability. In first few cycles, Nafion-212 membranes show lower coulombic efficiencies which gradually increased to 97.2%. This behavior is consistent with the literatures and attributed to the higher vanadium crossover rates in first few cycles [43, 44]. The low vanadium ion permeability can effectively prevent crossover/self-discharge, thus resulting in higher CE and reducing the need for frequent electrolyte rebalancing of VRFBs. The membranes

treated with lower concentrations of phosphoric acids do not swell the PBI matrix excessively, but clearly improve the electrochemical properties of membranes. The CE >99% for P/65/10 and P/25/5 over 100 cycles also indicates the chemical stability of the pre-treated PBI membranes in VRFBs.

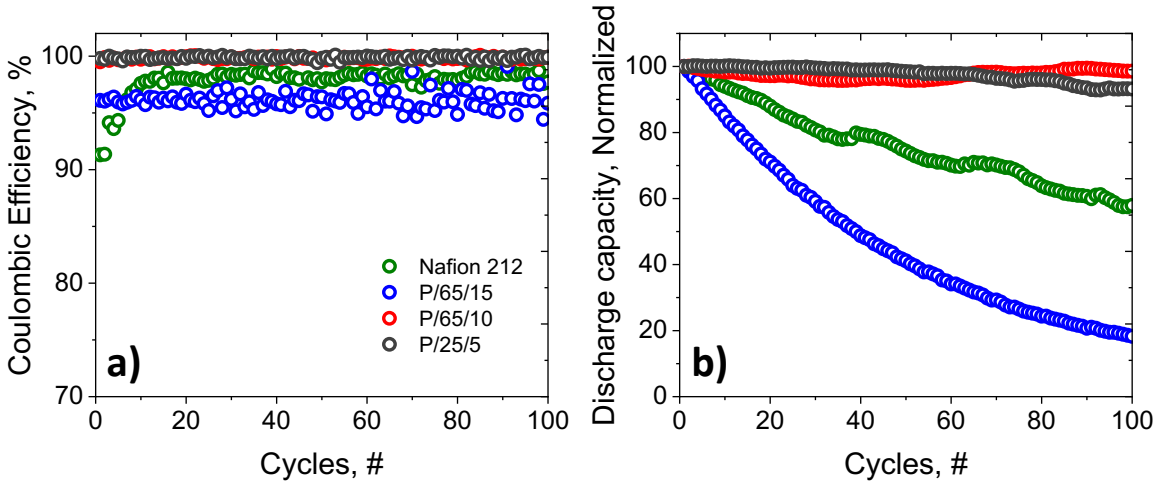

Figure 6. Coulombic efficiencies and discharge capacity decay of VRFBs assembled with Nafion-212, P/65/15, P/65/10 and P/25/5 membranes at 80 mA cm^{-2}.

The capacity decay rates of the P/65/15, P/65/10, P/25/5, and Nafion-212 membranes are shown in Fig. 6b. The P/65/15 membrane showed the highest capacity decay rate of 82% after 100 cycles due to the significantly high vanadium crossover. This result is in line with Peng et al., [35] who carried out the pre-treatment strategy with 85 wt% phosphoric acids (=15 M) and reported a 20% capacity loss in merely 20 cycles. The Nafion-212 showed the second worst capacity decay rate of 42.1% in merely 100 cycles, whereas P/65/10 and P/25/5 showed significantly lower capacity decay rates of 1.5 and 6.8%, respectively. Though, volume change and vanadium concentrations were not measured periodically, it was found that the cell using Nafion-212 observed 31% increase in the volume of negative electrolyte whereas no significant volume change was observed with P/65/10 and P/25/5 membranes. The normalized capacity for P/65/10 rose from 96% to 99% between 50 to 85 cycles which could be due to the difference in vanadium ions concentration in the cell caused by unequal crossover of different vanadium ion species [44]. Although it is tough to make an accurate comparison due to the different experimental conditions used in the literature, the capacity retention of the PBI membranes in this study is superior to those of the previously reported PBI membranes listed in Table 2. Our results presented in this work

demonstrate that the pre-treatment strategy can be optimized to enhance the properties of PBI membranes for VRFB applications.

Table 2. Energy efficiencies and capacity retention of PBI membranes reported in literature.

Type	Current density [mA cm^{-2}]	CE [%][a]	EE [%][a]	Capacity [Ah L^{-1} mol V^{-1}]	Capacity retention [%] in 100 cycles	Reference
Dense	**80**	**99.9 99.8**	**83.7 77.3**	**11.5 9.4**	**93.2 98.5**	**This work**
	200	99.5	89.0	8.5[f]	80.0	[45]
	140	99.0	86.5	9.2[d]	86.7	[46]
	140	99.0	88.5	10.7[d]	62.5	[47]
Composite	60	99.5	82.6	9.3[b]	88.0	[48]
	160	99.8	71.2	7.8[e]	74.7	[49]
Porous	160	99.2	83.2	4.4[e]	87.5	[50]
	120	99.5	87.9	9.7[c]	79.0	[34]
	80	98.9	90.1	15.6[a]	91.0	[51]
	80	99.1	82.0	11.6[a]	66.7 (50 cycles)	[42]

[a] Measured at 80 mA cm^{-2}, [b] Measured at 60 mA cm^{-2}, [c] Measured at 120 mA cm^{-2}, [d] Measured at 140 mA cm^{-2}, [e] Measured at 160 mA cm^{-2}, [f] Measured at 200 mA cm^{-2}

4. Conclusions:

In this study, a series of PBI membranes were prepared with phosphoric acid pretreatment. By adjusting the membrane thickness and phosphoric acid concentration, the electrochemical and physical properties of membranes were effectively controlled. Phosphoric acid pre-treatment swells the PBI matrix irreversibly; as a result, treated membranes show higher acid content and conductivity due to their increased free volume. The swelling of the PBI matrix increases the interaction of sulfuric acid with alkaline imidazole substructure and forms a positive charge on the PBI backbone, which further strengthens the Donnan exclusion effect and effectively prevents the crossover of positively charged Vanadium ions. Accordingly, high CE and excellent cycling performance can be achieved by VRFBs using PBI membranes. For instance, the P/25/5 membrane shows the CE and EE of 99.7-99.95%, and 68-90%, while achieving 18-40% higher discharge capacity compared to Nafion-212 between 40-200 mA cm^{-2}. Also, P/65/10, P/25/5, and Nafion-212 show capacity retention of 98.5, 93, and 58%, respectively. It translates to an outstanding 0.015, and 0.07% per cycle capacity decay rate for P/65/10 and P/25/5 membranes. This study not only provides a new strategy to fabricate highly selective and high-performance membranes based on PBI for VRFB at fraction of the cost of Nafion membrane but also indicates that PBI membranes

can be considered a promising alternative to commercial Nafion membranes for VRFB applications.

5. Acknowledgments

This work was supported by the Laboratory Directed Research and Development (LDRD) program of Los Alamos National Laboratory (LANL) under project number 20170046DR and 20210680ECR. The authors would like to thank Dr. Imre Gyuk and the U.S. Department of Energy, Office of Electricity for support in the publication of this work. Los Alamos National Laboratory is operated by Triad, LLC, for the National Nuclear Security Administration of the U.S. Department of Energy (Contract No. 89233218NCA000001).

6. References:

[1] M.V. Holland-Cunz, F. Cording, J. Friedl, U. Stimming, Redox flow batteries—Concepts and chemistries for cost-effective energy storage, Frontiers in Energy 12(2) (2018) 198-224. https://doi.org/10.1007/s11708-018-0552-4.

[2] M. Abdul Aziz, K. Oh, S. Shanmugam, A sulfonated poly(arylene ether ketone)/polyoxometalate–graphene oxide composite: a highly ion selective membrane for all vanadium redox flow batteries, Chemical Communications 53(5) (2017) 917-920. https://doi.org/10.1039/C6CC08855D.

[3] C. Minke, T. Turek, Economics of vanadium redox flow battery membranes, Journal of Power Sources 286 (2015) 247-257. https://doi.org/10.1016/j.jpowsour.2015.03.144.

[4] M.R. Ahmad Mayyas, Bryan Pivovar, Guido Bender, Keith Wipke, Manufacturing Cost Analysis for Proton Exchange Membrane Water Electrolyzers, 2019.

[5] T.L. Max Wei, Ahmad Mayyas, ShukHan Chan, David Gosselin, Hanna Breunig, Thomas McKone, A Total Cost of Ownership Model for High Temperature PEM Fuel Cells in Combined Heat and Power Applications, 2014.

[6] S. Zhang, B. Zhang, Y. Chen, X. Jian, Preparation and properties of quaternized poly (phthalazinone ether ketone ketone) anion-exchange membrane for all-vanadium redox flow battery, Kexue Tongbao/Chin. Sc. Bull. 64(2) (2019) 187-193. https://doi.org/10.1360/N972018-00776.

[7] Z. Yuan, X. Li, Y. Duan, Y. Zhao, H. Zhang, Highly stable membranes based on sulfonated fluorinated poly(ether ether ketone)s with bifunctional groups for vanadium flow battery application, Polymer Chemistry 6(30) (2015) 5385-5392. https://doi.org/10.1039/c5py00482a.

[8] B. Yin, Z. Li, W. Dai, L. Wang, L. Yu, J. Xi, Highly branched sulfonated poly(fluorenyl ether ketone sulfone)s membrane for energy efficient vanadium redox flow battery, Journal of Power Sources 285 (2015) 109-118. https://doi.org/10.1016/j.jpowsour.2015.03.102.

[9] S.W. Choi, T.H. Kim, S.W. Jo, J.Y. Lee, S.H. Cha, Y.T. Hong, Hydrocarbon membranes with high selectivity and enhanced stability for vanadium redox flow battery applications: Comparative study with sulfonated poly(ether sulfone)s and sulfonated poly(thioether ether sulfone)s, Electrochimica Acta 259 (2018) 427-439. https://doi.org/10.1016/j.electacta.2017.10.121.

[10] J. grosse Austing, C. Nunes Kirchner, L. Komsiyska, G. Wittstock, Layer-by-layer modification of Nafion membranes for increased life-time and efficiency of vanadium/air redox flow batteries, Journal of Membrane Science 510 (2016) 259-269. https://doi.org/10.1016/j.memsci.2016.03.005.

[11] S. Maurya, S.-H. Shin, Y. Kim, S.-H. Moon, A review on recent developments of anion exchange membranes for fuel cells and redox flow batteries, RSC Advances 5 (2015) 37206-37230. https://doi.org/10.1039/C5RA04741B.
[12] T. Wang, J.Y. Jeon, J. Han, J.H. Kim, C. Bae, S. Kim, Poly(terphenylene) anion exchange membranes with high conductivity and low vanadium permeability for vanadium redox flow batteries (VRFBs), Journal of Membrane Science 598 (2020) 117665. https://doi.org/https://doi.org/10.1016/j.memsci.2019.117665.
[13] E.J. Park, Y.S. Kim, Quaternized aryl ether-free polyaromatics for alkaline membrane fuel cells: synthesis, properties, and performance – a topical review, Journal of Materials Chemistry A 6(32) (2018) 15456-15477. https://doi.org/10.1039/C8TA05428B.
[14] A.D. Mohanty, S.E. Tignor, J.A. Krause, Y.-K. Choe, C. Bae, Systematic Alkaline Stability Study of Polymer Backbones for Anion Exchange Membrane Applications, Macromolecules 49(9) (2016) 3361-3372. https://doi.org/10.1021/acs.macromol.5b02550.
[15] X. Hao, N. Chen, Y. Chen, D. Chen, Accelerated degradation of quaternary ammonium functionalized anion exchange membrane in catholyte of vanadium redox flow battery, Polymer Degradation and Stability 197 (2022) 109864. https://doi.org/https://doi.org/10.1016/j.polymdegradstab.2022.109864.
[16] E.J. Park, S. Maurya, U. Martinez, Y.S. Kim, R. Mukundan, Quaternized poly(arylene ether benzonitrile) membranes for vanadium redox flow batteries, Journal of Membrane Science 617 (2021) 118565. https://doi.org/https://doi.org/10.1016/j.memsci.2020.118565.
[17] L. Wang, A.T. Pingitore, W. Xie, Z. Yang, M.L. Perry, B.C. Benicewicz, Sulfonated PBI Gel Membranes for Redox Flow Batteries, Journal of The Electrochemical Society 166(8) (2019) A1449-A1455. https://doi.org/10.1149/2.0471908jes.
[18] X. Shi, O.C. Esan, X. Huo, Y. Ma, Z. Pan, L. An, T.S. Zhao, Polymer Electrolyte Membranes for Vanadium Redox Flow Batteries: Fundamentals and Applications, Prog. Energy Combust. Sci. 85 (2021). https://doi.org/10.1016/j.pecs.2021.100926.
[19] J. Mader, L. Xiao, T.J. Schmidt, B.C. Benicewicz, Polybenzimidazole/Acid Complexes as High-Temperature Membranes, Fuel Cells II2008, pp. 63-124. https://doi.org/10.1007/12_2007_129.
[20] M.R. Berber, N. Nakashima, Tailoring Different Molecular Weight Phenylene–Polybenzimidazole Membranes with Remarkable Oxidative Stability and Conductive Properties for High-Temperature Polymer Electrolyte Fuel Cells, ACS Applied Materials & Interfaces 11(49) (2019) 46269-46277. https://doi.org/10.1021/acsami.9b18314.
[21] X.L. Zhou, T.S. Zhao, L. An, L. Wei, C. Zhang, The use of polybenzimidazole membranes in vanadium redox flow batteries leading to increased coulombic efficiency and cycling performance, Electrochimica Acta 153 (2015) 492-498. https://doi.org/10.1016/j.electacta.2014.11.185.
[22] L. Ding, X. Song, L. Wang, Z. Zhao, G. He, Preparation of dense polybenzimidazole proton exchange membranes with different basicity and flexibility for vanadium redox flow battery applications, Electrochimica Acta 292 (2018) 10-19. https://doi.org/10.1016/j.electacta.2018.08.128.
[23] D. Chen, H. Qi, T. Sun, C. Yan, Y. He, C. Kang, Z. Yuan, X. Li, Polybenzimidazole membrane with dual proton transport channels for vanadium flow battery applications, Journal of Membrane Science 586 (2019) 202-210. https://doi.org/10.1016/j.memsci.2019.05.076.
[24] Y. Lee, S. Kim, A. Maljusch, O. Conradi, H.-J. Kim, J.H. Jang, J. Han, J. Kim, D. Henkensmeier, Polybenzimidazole membranes functionalised with 1-methyl-2-mesitylbenzimidazolium ions via a hexyl linker for use in vanadium flow batteries, Polymer 174 (2019) 210-217. https://doi.org/10.1016/j.polymer.2019.04.048.
[25] L. Ding, X. Song, L. Wang, Z. Zhao, Enhancing proton conductivity of polybenzimidazole membranes by introducing sulfonate for vanadium redox flow batteries applications, Journal of Membrane Science 578 (2019) 126-135. https://doi.org/10.1016/j.memsci.2019.02.050.

[26] M. Jung, W. Lee, N. Nambi Krishnan, S. Kim, G. Gupta, L. Komsiyska, C. Harms, Y. Kwon, D. Henkensmeier, Porous-Nafion/PBI composite membranes and Nafion/PBI blend membranes for vanadium redox flow batteries, Applied Surface Science 450 (2018) 301-311. https://doi.org/10.1016/j.apsusc.2018.04.198.
[27] M. Jung, W. Lee, C. Noh, A. Konovalova, G.S. Yi, S. Kim, Y. Kwon, D. Henkensmeier, Blending polybenzimidazole with an anion exchange polymer increases the efficiency of vanadium redox flow batteries, Journal of Membrane Science 580 (2019) 110-116. https://doi.org/10.1016/j.memsci.2019.03.014.
[28] E. Bülbül, V. Atanasov, M. Mehlhorn, M. Bürger, A. Chromik, T. Häring, J. Kerres, Highly phosphonated polypentafluorostyrene blended with polybenzimidazole: Application in vanadium redox flow battery, Journal of Membrane Science 570-571 (2019) 194-203. https://doi.org/https://doi.org/10.1016/j.memsci.2018.10.027.
[29] W. Lee, M. Jung, D. Serhiichuk, C. Noh, G. Gupta, C. Harms, Y. Kwon, D. Henkensmeier, Layered composite membranes based on porous PVDF coated with a thin, dense PBI layer for vanadium redox flow batteries, Journal of Membrane Science 591 (2019). https://doi.org/10.1016/j.memsci.2019.117333.
[30] L. Gubler, D. Vonlanthen, A. Schneider, F.J. Oldenburg, Composite Membranes Containing a Porous Separator and a Polybenzimidazole Thin Film for Vanadium Redox Flow Batteries, Journal of The Electrochemical Society 167(10) (2020). https://doi.org/10.1149/1945-7111/ab945f.
[31] J.C. Duburg, K. Azizi, S. Primdahl, H.A. Hjuler, E. Zanzola, T.J. Schmidt, L. Gubler, Composite Polybenzimidazole Membrane with High Capacity Retention for Vanadium Redox Flow Batteries, Molecules 26(6) (2021). https://doi.org/10.3390/molecules26061679.
[32] S. Maurya, S.-H. Shin, J.-Y. Lee, Y. Kim, S.-H. Moon, Amphoteric nanoporous polybenzimidazole membrane with extremely low crossover for a vanadium redox flow battery, RSC Advances 6(7) (2016) 5198-5204. https://doi.org/10.1039/c5ra26244e.
[33] L. Zeng, Y. Ren, L. Wei, X. Fan, T. Zhao, Asymmetric Porous Polybenzimidazole Membranes with High Conductivity and Selectivity for Vanadium Redox Flow Batteries, Energy Technol. 8(10) (2020). https://doi.org/10.1002/ente.202000592.
[34] X. Che, H. Zhao, X. Ren, D. Zhang, H. Wei, J. Liu, X. Zhang, J. Yang, Porous polybenzimidazole membranes with high ion selectivity for the vanadium redox flow battery, Journal of Membrane Science 611 (2020). https://doi.org/10.1016/j.memsci.2020.118359.
[35] S. Peng, X. Yan, D. Zhang, X. Wu, Y. Luo, G. He, A H3PO4 preswelling strategy to enhance the proton conductivity of a H2SO4-doped polybenzimidazole membrane for vanadium flow batteries, RSC Advances 6(28) (2016) 23479-23488. https://doi.org/10.1039/c6ra00831c.
[36] S. Maurya, P.T. Nguyen, Y.S. Kim, Q. Kang, R. Mukundan, Effect of flow field geometry on operating current density, capacity and performance of vanadium redox flow battery, Journal of Power Sources 404 (2018) 20-27. https://doi.org/https://doi.org/10.1016/j.jpowsour.2018.09.093.
[37] X. Glipa, B. Bonnet, B. Mula, D. J. Jones, J. Rozière, Investigation of the conduction properties of phosphoric and sulfuric acid doped polybenzimidazole, Journal of Materials Chemistry 9(12) (1999) 3045-3049. https://doi.org/10.1039/A906060J.
[38] C. Noh, M. Jung, D. Henkensmeier, S.W. Nam, Y. Kwon, Vanadium Redox Flow Batteries Using meta-Polybenzimidazole-Based Membranes of Different Thicknesses, ACS Applied Materials and Interfaces 9(42) (2017) 36799-36809. https://doi.org/10.1021/acsami.7b10598.
[39] J.-K. Jang, T.-H. Kim, S.J. Yoon, J.Y. Lee, J.-C. Lee, Y.T. Hong, Highly proton conductive, dense polybenzimidazole membranes with low permeability to vanadium and enhanced H2SO4absorption capability for use in vanadium redox flow batteries, J. Mater. Chem. A 4(37) (2016) 14342-14355. https://doi.org/10.1039/c6ta05080h.

[40] T. Wang, S.J. Moon, D.-S. Hwang, H. Park, J. Lee, S. Kim, Y.M. Lee, S. Kim, Selective ion transport for a vanadium redox flow battery (VRFB) in nano-crack regulated proton exchange membranes, Journal of Membrane Science 583 (2019) 16-22. https://doi.org/10.1016/j.memsci.2019.04.017.
[41] F.G. Donnan, Theory of membrane equilibria and membrane potentials in the presence of non-dialysing electrolytes. A contribution to physical-chemical physiology, Journal of Membrane Science (100) (1995) 45-55. https://doi.org/https://doi.org/10.1016/0376-7388(94)00297-C.
[42] S. Peng, X. Yan, X. Wu, D. Zhang, Y. Luo, L. Su, G. He, Thin skinned asymmetric polybenzimidazole membranes with readily tunable morphologies for high-performance vanadium flow batteries, RSC Advances 7(4) (2017) 1852-1862. https://doi.org/10.1039/c6ra24801b.
[43] E. Lallo, A. Khataee, R.W. Lindström, Vanadium Redox Flow Battery Using Aemion™ Anion Exchange Membranes, Processes 10(2) (2022) 270.
[44] J.H. Park, J.J. Park, O.O. Park, J.H. Yang, Capacity Decay Mitigation by Asymmetric Positive/Negative Electrolyte Volumes in Vanadium Redox Flow Batteries, ChemSusChem 9(22) (2016) 3181-3187. https://doi.org/https://doi.org/10.1002/cssc.201601110.
[45] S.-W.J. Jung-Kyu Jang, Jun Woo Jeon, Byoung Gak Kim, Sang Jun Yoon, Duk Man Yu, Young Taik Hong, Hee-Tak Kim, Tae-Ho Kim, Alkyl Spacer Grafted ABPBI Membranes with Enhanced AcidAbsorption Capabilities for Use in Vanadium Redox Flow Batteries, ACS Appl. Ener. Mat. 4 (2021) 4672-4685. https://doi.org/10.1021/acsaem.1c00280.
[46] K. Geng, Y. Li, Y. Xing, L. Wang, N. Li, A novel polybenzimidazole membrane containing bulky naphthalene group for vanadium flow battery, Journal of Membrane Science 586 (2019) 231-239. https://doi.org/10.1016/j.memsci.2019.05.062.
[47] S. Peng, X. Wu, X. Yan, L. Gao, Y. Zhu, D. Zhang, J. Li, Q. Wang, G. He, Polybenzimidazole membranes with nanophase-separated structure induced by non-ionic hydrophilic side chains for vanadium flow batteries, Journal of Materials Chemistry A 6(9) (2018) 3895-3905. https://doi.org/10.1039/c7ta08790j.
[48] S.M. Ahn, H.Y. Jeong, J.-K. Jang, J.Y. Lee, S. So, Y.J. Kim, Y.T. Hong, T.-H. Kim, Polybenzimidazole/Nafion hybrid membrane with improved chemical stability for vanadium redox flow battery application, RSC Advances 8(45) (2018) 25304-25312. https://doi.org/10.1039/c8ra03921f.
[49] F.J. Oldenburg, E. Nilsson, T.J. Schmidt, L. Gubler, Tackling Capacity Fading in Vanadium Redox Flow Batteries with Amphoteric Polybenzimidazole/Nafion Bilayer Membranes, ChemSusChem 12(12) (2019) 2620-2627. https://doi.org/10.1002/cssc.201900546.
[50] L. Ding, Y. Wang, L. Wang, X. Han, Microstructure regulation of porous polybenzimidazole proton conductive membranes for high-performance vanadium redox flow battery, Journal of Membrane Science 642 (2022). https://doi.org/10.1016/j.memsci.2021.119934.
[51] Z. Yuan, Y. Duan, H. Zhang, X. Li, H. Zhang, I. Vankelecom, Advanced porous membranes with ultra-high selectivity and stability for vanadium flow batteries, Energy & Environmental Science 9(2) (2016) 441-447. https://doi.org/10.1039/c5ee02896e.